Anat Embryol (2005) 210: 245–263
DOI 10.1007/s00429-005-0048-y

ORIGINAL ARTICLE

Erh-Fang Lee · Russell E. Jacobs · Ivo Dinov
Alex Leow · Arthur W. Toga

Standard atlas space for C57BL/6J neonatal mouse brain

Accepted: 9 August 2005 / Published online: 14 October 2005

Abstract A standard atlas space with stereotaxic co-ordinates for the postnatal day 0 (P0) C57BL/6J mouse brain was constructed from the average of eight individual co-registered MR image volumes. Accuracy of registration and morphometric variations in structures between subjects were analyzed statistically. We also applied this atlas coordinate system to data acquired using different imaging protocols as well as to a high-resolution histological atlas obtained from separate animals. Mapping accuracy in the atlas space was examined to determine the applicability of this atlas framework. The results show that the atlas space defined here provides a stable framework for image registration for P0 normal mouse brains. With an appropriate feature-based co-registration strategy, the probability atlas can also provide an accurate anatomical map for images acquired using invasive imaging methods. The atlas templates and the probability map of the anatomical labels are available at http://www.loni.ucla.edu/MAP/.

Keywords Mouse atlas · Stereotaxic co-ordinate · Feature-based registration · Anatomical morphometry · MR imaging · Gene expression mapping · Developing brain

Abbreviations P0: Postnatal day 0 · SD: Standard deviation

E.-F. Lee · I. Dinov · A. Leow · A. W. Toga (✉)
Department of Neurology, Laboratory of Neuro Imaging,
Reed Neurological Research Center, UCLA School of Medicine,
Room 4238, 710 Westwood Plaza, Los Angeles,
CA 90095-1769, USA
E-mail: toga@loni.ucla.edu
Tel.: +1-310-2062101
Fax: +1-310-2065518

R. E. Jacobs
Beckman Institute, California Institute of Technology,
1200 E. California Blvd., Pasadena, CA 91125, USA

Introduction

Most brain atlases facilitate structural mapping by providing stereotaxic coordinates that define brain orientations and positions with grid systems. As the anatomical space is described with a common numerical system, the coordinate representation also can serve as an index for database entries facilitating integration of multimodality data based on their spatial relationships. To date, however, no published atlas for the developing mouse brain includes a coordinate system (Schambra et al. 1992; Jacobowitz and Abbott 1998; Baldock et al. 2001). As genes involved in morphogenesis and functional development usually have specific spatial expression patterns, a coordinate system for each development stage is required to correlate the gene expression and the brain anatomy. In this study, we focus on constructing an atlas for the Postnatal day 0 (P0) mouse brain with a coordinate system. Data from this time point are often collected in studies that monitor the temporal process of cell differentiation or the changes of gene expression patterns (e.g., Diep et al. 2004 (prenatal development); Parras et al. 2004 (postnatal development); Gray et al. 2004 (both prenatal and postnatal)). As the anatomical structures are presented within a standard space, the atlas provides a framework for data repository. A standard framework also facilitates data comparison and consistency between different laboratories.

In most adult rodent brain atlases, reference markers made by inserting pins through the skull from the bony landmarks Lambda and Bregma (Paxinos and Franklin 2001; Swanson 1998) define the coordinate system. The coordinate scale defined by the in vivo distance between these markers thus enables the atlas to reference the native brain space. However, due to incomplete bone calcification at P0, the spatial relationship between brain and skull is inconsistent. Hence, the markers referenced with the bony landmarks in adult rodent atlases are unreliable for the definition of a coordinate system for the developing mouse brain. In addition, because the

brain grows quickly at early development stages, variations in structures between individuals are larger than in fully developed brains. A coordinate system that permits the localization of the brain structures regardless of the shape and size of the brain is required. This kind of coordinate system is usually defined with internal structures whose spatial integrity is well preserved. For example, the line joining the anterior commissure (AC) and posterior commissure (PC) helps to define the scale of the brain in the Talairach and Tournoux coordinate system of the human atlas (Talairach and Tournoux 1988). Therefore, we used internal anatomical structures to define the coordinate system for the P0 mouse brain atlas. Image volumes obtained from non-invasive MR scanning provided undistorted image data of anatomical structures, and the resolution is sufficient to identify several important internal landmarks. Hence, we used MR image volumes to define the atlas space.

Due to the morphological variation at P0, the coordinate system determined by a single animal used for the brain atlas of the adult lab rodent cannot present a stable framework for the developing mouse brains. Human and some animal atlases for brains that are highly various across population have been generated by co-registering data from different subjects (Watanabe et al. 2001; Mazziotta et al. 2001; Thompson et al. 2002; Kovacevic et al. 2004). The coordinates for the brains are then defined based on the average space. Such atlases provide the power to statistically represent a population. By using an average space of the co-registered brain image volumes acquired from eight normal P0 mice (two sets of littermates) as the basis for our atlas, we account for the brain diversity of a normal population at P0. Coordinate values were assigned according to the co-registered average brain in order to avoid capturing any geometrical outlier. Statistical morphometric analysis was performed to evaluate the variations in the atlas space. The resulting coordinate system also maintains a spatial range for several important anatomical structures in probability, indicating confidence levels of mapping accuracy for the structure at each coordinate. In addition to being an anatomical map, the anatomical labels based on the average brain provide a template to facilitate a modality-independent, atlas-based registration. Accuracy of the atlas space was examined using the data acquired from animals not used to construct the atlas.

At P0, the basic architecture of the cerebrum, midbrain, hindbrain, and brainstem are consistent with the adult brain. As the anatomical structures were presented with numerical coordinates, the atlas can quantitatively relate to the brain anatomy of later development stages and provide an important reference for those maturational morphological changes.

Materials and methods

Constructing the standard atlas space

In this section, we describe how the coordinate for the atlas was defined, how the brain image for the atlas was established, and how the probability anatomical maps were calculated.

Coordinate definition

We designed a grid system that consistently orients and positions the P0 brains. We assigned the origin (O) to be the posterior end of interpeduncular fossa on the medial sagittal plane (Fig. 1). The line passing through the origin and the intersection of the rhinal fissure and the cerebral longitudinal fissure (I) defines the *y*-axis for our coordinate system. These two points (O and I) were selected as reference landmarks as they are easily visible in most image data, generally well preserved during sample preparation, and posses little geometrical variation throughout development. It has been shown that the brain space is presented more accurately if more of the area of interest is encompassed by the reference system (Rehm et al. 2000; Li et al. 2004). The two points (O and I) used for axial reference are located on the boundary of the forebrain (cerebrum plus diencephalon); hence, the distance between them is long enough to align the brain with little variation. The *z*-axis is the line perpendicular to *y* on the mid-sagittal plane passing through the origin, and the *x*-axis is described as the line perpendicular to *y* and *z* axes and passing through the origin.

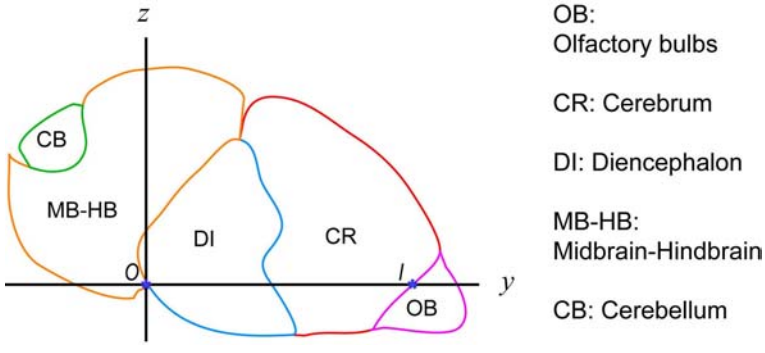

Fig. 1 Reference points on the mid-sagittal plane used to define the neonatal coordinate system. *O* the posterior end of interpeduncular fossa plane, *I* the intersection of the rhinal fissure and the cerebral longitudinal fissure

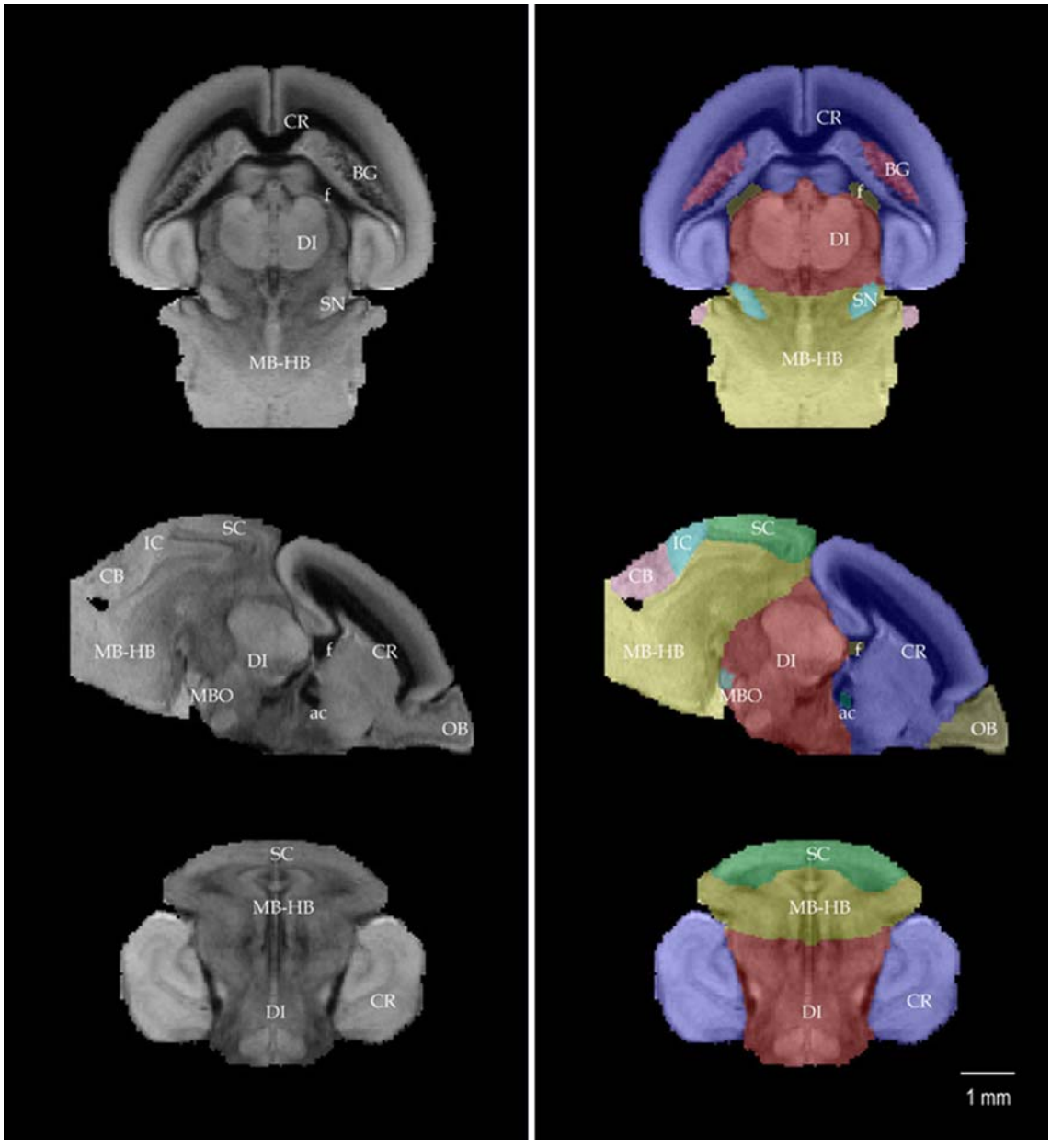

Fig. 2 Anatomical labels on the MR image volume. Each MR brain image volume was segmented into olfactory bulbs (*OB*), cerebrum (*CR*), diencephalon (*DI*), midbrain–hindbrain (MB–HB), and cerebellum (*CB*) as in Fig. 1 to facilitate the morphometric analysis. Structures with clearer boundaries: temporal limb of the anterior commissure (*AC*), fimbria of the hippocampus (*f*), basal ganglia (*BG*), mammillary body (*MBO*), superior colliculus (*SC*), inferior colliculus (*IC*), and substantia nigra (*SN*), were also delineated. *Left column* shows one of the raw MR images used to construct the atlas. *Right column* shows the anatomical labels overlapping. This brain was used as the registration target at the first step of registration (see Materials and methods section). *Rows* from top to bottom: the horizontal, sagittal, and coronal views

MR image acquisition

Eight mice from two sets of littermates were sacrificed hypothermally within 24 h after birth. After intracardial perfusion with 10 ml of phosphate-buffered saline (PBS) and then 10 ml 2% paraformaldehyde (PFA), the animals were decapitated and the heads postfixed with 2% PFA for 24 h before MR scans. Heads were soaked in 5% ProHance® (paramagnetic MR contrast agent) for 5 days then immersed in Fomblin® (an embedding medium to limit tissue dehydration) for the MR scans. T2-weighted 3D spin-echo MRI images were acquired using an 11.7 T BrukerAvance imaging spectrometer with a micro-imaging gradient insert and 20 mm birdcage RF coil (Bruker Instruments). The following data acquisition parameters were used: TR/TE = 300/6.8 ms, two averages, FOV = 12.8×9×9 mm^3, matrix size = 256×128×128, T = 288.1 K. Spatial resolution of the obtained images was 70 ×50×70 μm^3 per voxel or 40×40×40 μm^3 per voxel. The mice weighed between 1.4 and 1.5 g before being

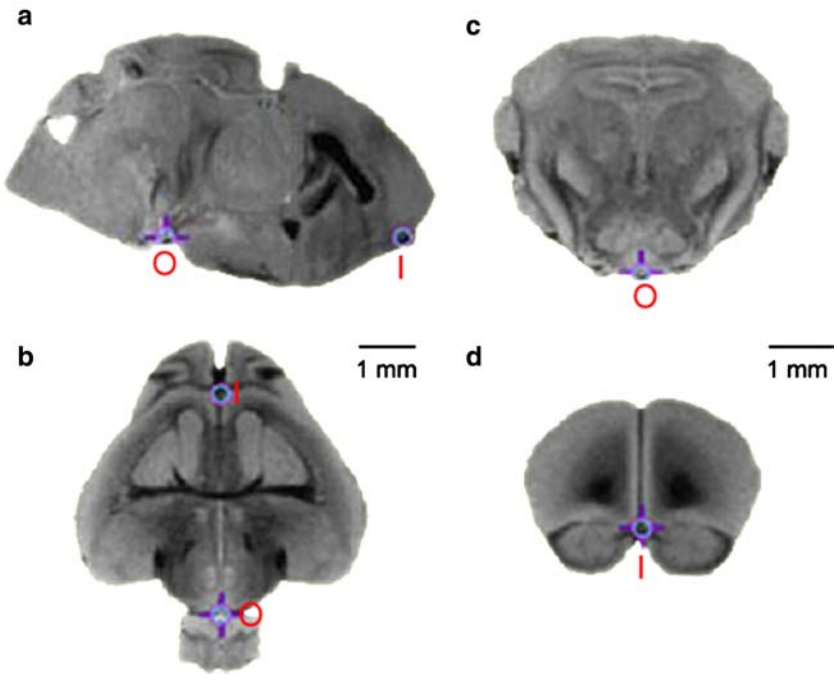

Fig. 3 a–d The reference points used to define the coordinate system of a MR image volume. Locations of points are shown in the three orthogonal planes. **a** sagittal plane, **b** horizontal plane, **c** and **d** coronal planes. *O* Origin, the posterior end of the interpeduncular fossa on the mid-sagittal plane. *I* the intersection of the rhinal fissure and the cerebral longitudinal fissure

sacrificed. All animals were housed and treated in accordance with the UCLA Animal Research Committee guidelines.

Tissue labeling for raw MR images

Each MR brain image volume was first segmented into olfactory bulbs, cerebrum, diencephalon, midbrain—hindbrain, and cerebellum as in Fig. 1. The basal ganglia (including only caudate putamen + globus pallidus), mammillary bodies, superior and inferior colliculi, substantia nigra, and white matter tracts AC (temporal limb) and fimbria of hippocampus, were then labeled. The primary reference for delineation was the adult mouse brain atlas of Paxinos and Franklin (2001). The neuroanatomy at age P0 is similar but not identical to the adult mouse brain. These structures were delineated because their boundaries could be identified clearly in all eight raw MR volumes. Nomenclature for each anatomical label was assigned to the structure best representing the delineation (name of smallest structure including all the painted nuclei) and was consistent with what we used in the adult mouse atlas (MacKenzie-Graham et al. 2004). Since some substructures were unrecognizable, we only labeled regions with clear boundaries in basal ganglia and AC and indicated which sub-nuclei were included in the parenthesis. Labeling was done manually using in-house software Duff (Shattuck et al. 2004). This program allows the user to view simultaneously all three orthogonal planes and "paint" on volumes, effectively labeling every voxel. Each label was assigned an intensity value uniquely referencing to the anatomic structures (Fig. 2). These anatomical labels are also used for feature-based co-registration.

Atlas space construction

An average brain of co-registered image volume was calculated for the P0 atlas. Each image volume was registered to a common space with four steps. Initial alignment employed a six-parameter linear rigid body transformation (rotation and translation only) to fix the location of the origin (O, interpeduncular fossa) and orient the brain such that the points O and I (the intersection of the rhinal fissure and the cerebral longitudinal fissure) simultaneously localized on the horizontal plane and the medial sagittal plane (Figs. 1, 3). The line that connects point O and I defines the *y*-axis of the coordinate system. The secondary registration was accomplished with a 12-parameter affine transformation calculated using an automatic registration algorithm that maximizes 3D cross-correlation of the image intensity (Woods et al. 1993). The image volume that retained the best structural integrity and the best image contrast was selected as the registration target for the other seven image volumes. Regions outside the brains were masked before the automatic registration step was performed. This second registration step normalized the global scale. Histogram equalization was performed on the resulting images. The intensity average brain of these eight co-registered images was then created. Histogram equalization prevented an average image from being biased toward the brighter image, and thus represents an average space of the co-registered brains. This average brain then served as the new target for registration step three. Here, a 30-parameter nonlinear warping was used to reduce regional variations between subjects (Woods et al. 1993). Finally, a feature-based registration was performed to

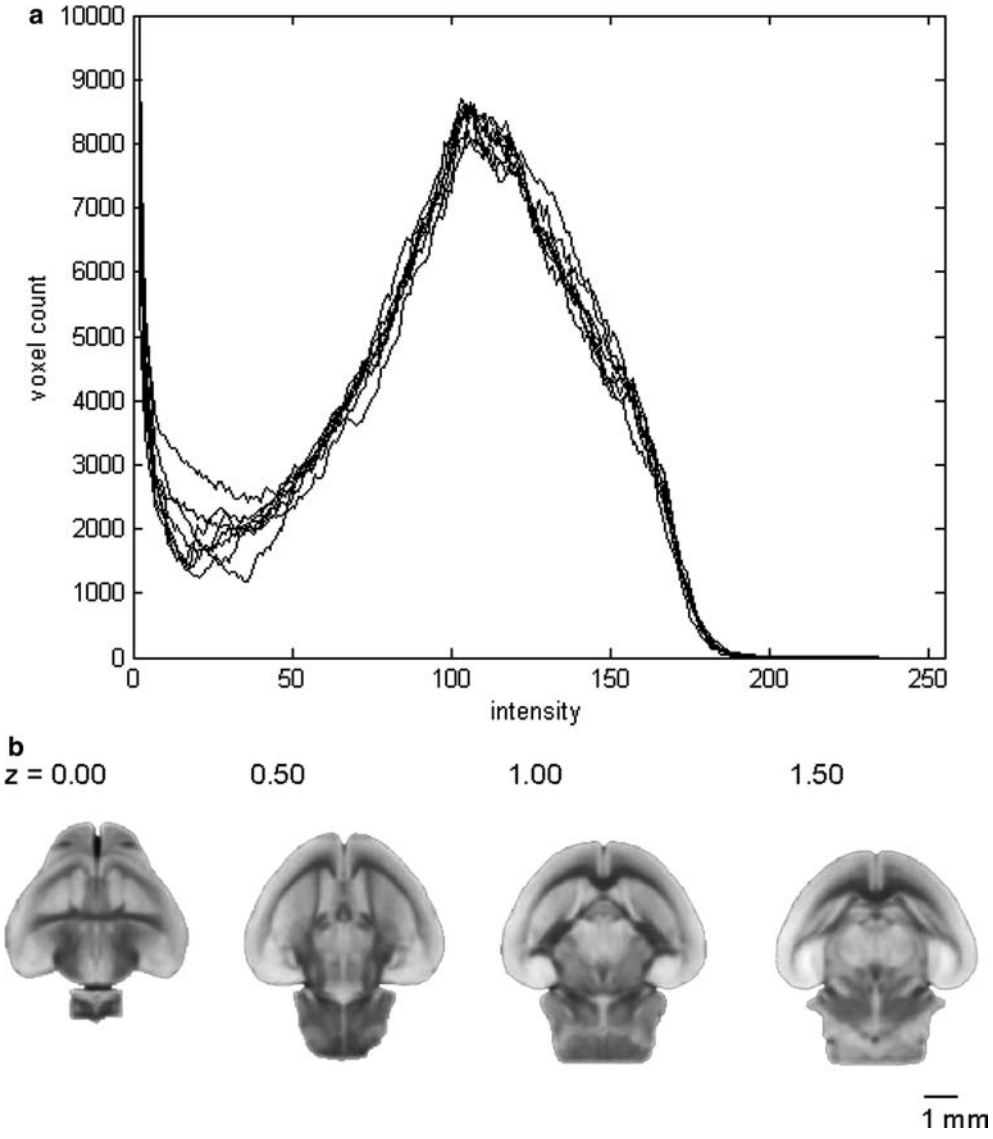

Fig. 4 **a** Homogeneous histograms for all eight brains used to construct the atlas space guarantee that the average intensity of the brains is not biased toward the brighter individuals. **b** Selected horizontal views of the average brain at $z = 0.0$, 0.5, 1.0, and 1.5 mm. The average brain is the average intensity of the eight co-registered brains. Three orthogonal planes with coordinate values are shown

maximize the mutual information between the anatomical label volume of each subject and the label volume drawn on the intensity average volume from the eight co-registered brains. Retrieved displacement fields were then used to resample each image volume (Leow et al. 2005). A newly averaged image of these eight-revised co-registered brain forms the standard atlas space.

Mophometric analysis

Each anatomical label was exported as an individual image volume. The volumes and the center-of-masses of these label volumes were used to evaluate geometrical variations of the brain space before and after co-registering. To facilitate the voxel-by-voxel analysis, all structural label volumes were resampled to isotropic volumes with a final resolution of 0.05×0.05×0.05 mm. Measurements were performed in the voxel space. All structure label volumes were resampled to the standard atlas space using the displacement fields that were used to bring the images from native space to the defined standard atlas space.

Defining the probability maps

The probability map indicates the confidence level of the anatomical space for each structure. We used the method described in Watanabe et al. (2001) and Chiavaras et al. (2001) to define the probability map. In brief, the volumes of the anatomical labels were superimposed. To calculate the probability maps of the native and atlas space, we used the resulting labels from the six parameter and the subsequent feature-based co-registration, respectively. The incidence that each spatial coordinate was occupied by any of the delineated anatomical structures was used to calculate these probabilities. Each voxel in the probability map for a given anatomical structure, therefore, describes the probability that the voxel belongs to this anatomical structure. The

label volume retrieved from a given threshold is the collection of voxels with probabilities greater than the threshold.

Anatomical labeling on the average brain

Labeling on the average brain generated the anatomical map for the atlas. The resulting labeled brain also served as the anatomical template for atlas-based registration. Since the atlas brain was the intensity average of the co-registered brains, boundaries of some structures might not be as clear as those of the raw MR image. To present a confident anatomical space, the anatomical labels were expanded from the labels retrieved from the probability maps with the threshold at 62.5%. The retrieved volumes at this threshold were close to, but less than the population average. These labels were slightly smaller than the actual sizes of the corresponding structures,

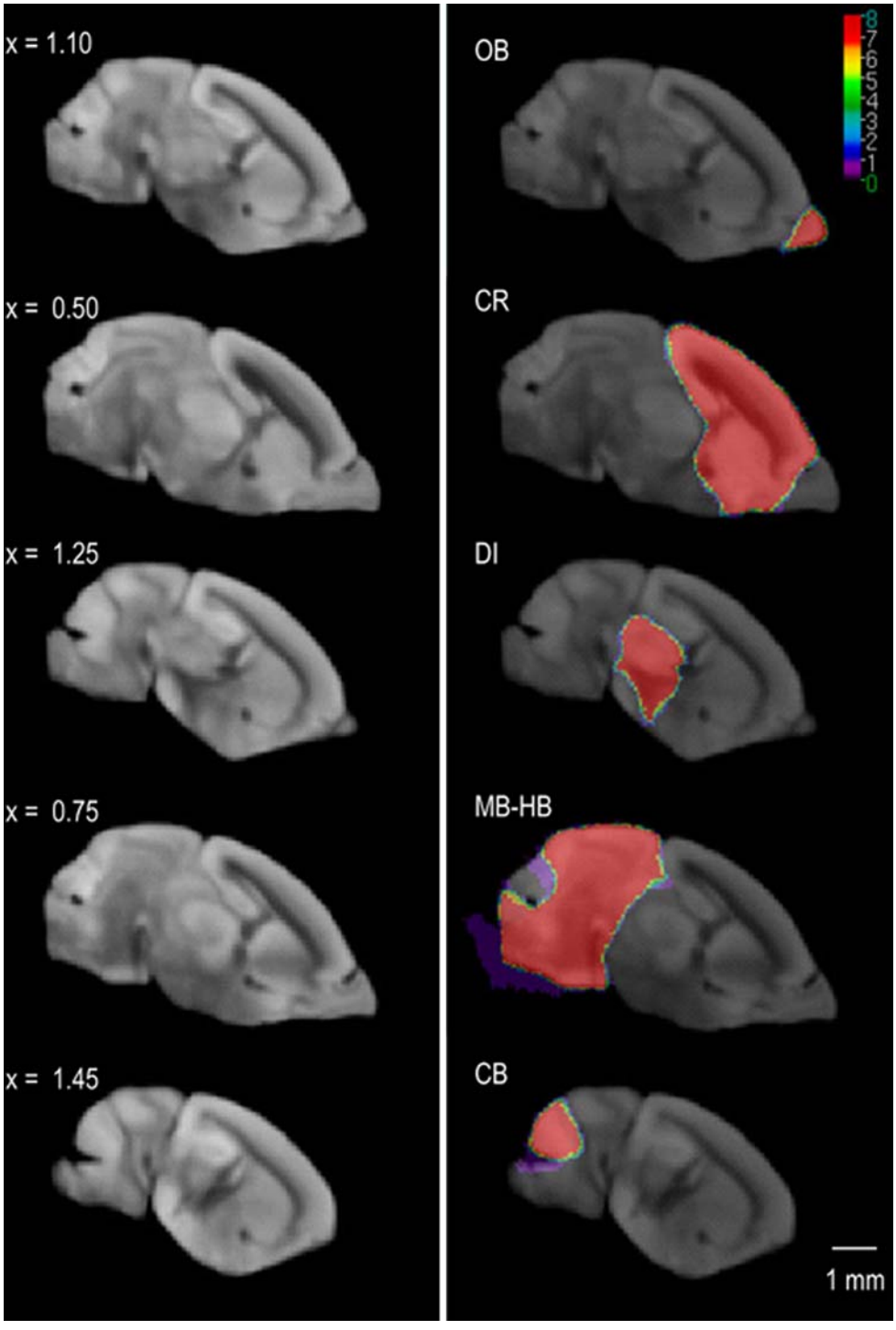

Fig. 5 **a** Probability maps of olfactory bulbs (*OB*), cerebrum (*CR*), diencephalon (*DI*), midbrain–hindbrain (MB–HB), and cerebellum (*CB*) (saggital views). *Left column* shows the image of the atlas brain, and the *right column* shows the images with the probability maps overlapping. The *colors* indicate the incidents of the structure appearing at a coordinate in the eight co-registered brains used to generate the atlas. **b** Probability maps of basal ganglia (*BG*), temporal limb of anterior commissure (*AC*), and fimbria of hippocampus (*f*) in cerebrum, mammillary body (*MBO*) in diencephalon, substantia migra (*SN*), superior colliculus (*SC*), and inferior colliculus (*IC*) in the minbrain–hindbrain after co-registration (coronal views). *Left column* shows the image of the atlas brain, and the *right column* shows the images with the probability maps overlapping on it. The *colors* indicate the incidents of the structure appearing at a coordinate in the eight co-registered brains used to generate the atlas

Fig. 5 (Contd.)

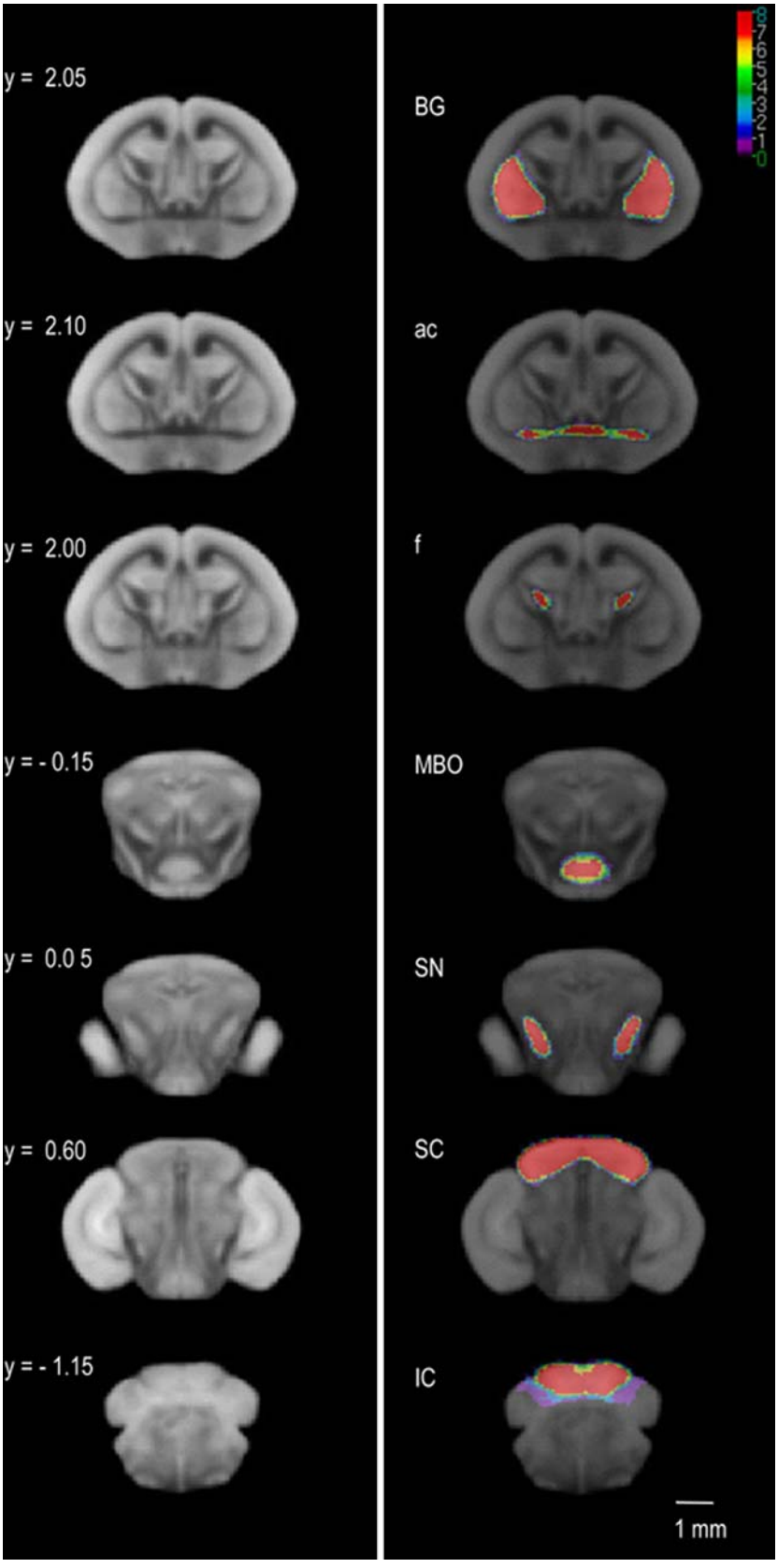

resulting in gaps along the boundaries between neighbor structures. These gaps were filled manually based on the intensity of the average image. If the boundary could not be easily discriminated on the image, delineations were made along the midpoints between boundaries defined by labels retrieved from the probability map.

Application

We used a T1-weighted MR image and a reconstructed histological image volume to examine the generalization of the atlas space. The atlas image and anatomical labels served as the template for registration. The matching test examined the mapping accuracy of each anatomic label.

Processing of test MR image

A T1-weighted MR image volume acquired from another P0 mouse was used as a test brain. This brain was processed using a different protocol than the one we adopted to prepare the brain for the atlas (longer fixation time with 2% PFA). We used this data to test whether the atlas space we defined is applicable for data prepared with a different protocol but which preserved its spatial integrity. The brain was first co-registered to the atlas using a 12-parameter transformation (Woods et al. 1993). The atlas brain image served as the registration target for the first step of normalization. Anatomical structures were then labeled on the test brain using the atlas as the reference. The boundaries of the structures delineated in the atlas were recognizable in most regions of the T1-weighted MR volume (Fig. 7). If the boundaries could not be clearly discriminated, the structures were delineated based on the relative position of the surrounding structures and the structures' 3D atlas morphology. Feature-based warping was then performed to maximize the mutual information between the anatomical labels of the test brain and those in the atlas (Leow et al. 2005).

Processing of histological images

We also used a previously generated histological image volume to examine the generalization of the atlas spaces defined by the co-registered MR brains. One animal of age P0 was used to generate the histological images for reconstructing the whole brain. The animal was sacrificed and perfused using a similar protocol as those animals used for the atlas. The whole brain was then postfixed with 2% PFA for 2 days, then cryoprotected with sucrose solutions increasing from 15 to 30%. Still within the skull, the brain was embedded in OCT compound (Sakura) and frozen at −70°C in ethanol/dry ice bath. Coronal sections (plane perpendicular to longitudinal axis) of 25 μm thickness were collected serially on a cryostat. Nissl-staining was performed on alternative sections. Stained preparations were digitized using a 1.25 times objective on an AX70 microscope (Olympus) with a DMX-1200 digital camera (Nikon) at a resolution of 3840×3072 (approximately 1.78 μm/pixel) in 24-bit color. Images of stained sections were first brought into registration using a rigid body transformation with software called Baladin (Ourselin et al. 2001). We then created the reference images by registering a MRI volume to the registered stained-image volume using a nine-

Table 1 Dimensions (mean ± SD in mm) and volumes (mean ± SD in mm^3) of the brain of the anatomical structures in the native and atlas spaces

Scales in each dimension (mm)				
	Native	Atlas	*t*-test *p*-value	*F*-test *p*-value
Maximum × dimension	6.30 ± 0.12	6.18 ± 0.05	0.0408	0.0195
Height of pineal gland (*Z*)	1.97 ± 0.22	1.69 ± 0.09	0.1525	0.0018
Length of OI line (*Y*)	4.15 ± 0.16	4.24 ± 0.04	0.0022	0.0164
The volumes of the anatomical labels (mm^3) as shown in Fig. 1				
Structure	Native space	Atlas space	*t*-test *p*-value	*F*-test *p*-value
Olfactory bulbs	2.18 ± 0.25	2.13 ± 0.11	0.6133	0.0199
Cerebrum	48.11 ± 3.31	48.59 ± 0.53	0.7000	0.0000
Basal ganglia left	1.91 ± 0.17	2.23 ± 0.15	0.0007	0.3572
Basal ganglia right	1.84 ± 0.16	2.16 ± 0.11	0.0010	0.1998
Diencephalon	12.83 ± 0.81	13.32 ± 0.21	0.0812	0.0010
Mammillary body	0.16 ± 0.06	0.14 ± 0.04	0.1234	0.2217
Midbrain–hindbrain	25.56 ± 1.46	24.85 ± 1.62	0.3542	0.6020
Substantia nigra left	0.123 ± 0.03	0.14 ± 0.02	0.5625	0.1524
Substantia nigra right	0.13 ± 0.03	0.14 ± 0.02	0.6663	0.0680
Superior colliculus	3.11 ± 0.23	3.19 ± 0.24	0.4650	0.5279
Inferior colliculus	1.75 ± 0.24	1.82 ± 0.11	0.5136	0.0311
Cerebellum	3.82 ± 0.37	3.92 ± 0.25	0.5394	0.1733
Whole brain	92.50 ± 5.70	92.82 ± 2.21	0.8855	0.0115

Paired *t*-tests were performed to test the null hypothesis that the values in the native space are equal to those in the atlas space. *F*-tests were also performed to test the null hypothesis that the variances in the atlas space are less than those in the native space, *df* (7,7)

Table 2 Center-of-masses of the anatomic structures in the atlas space

	Distance from the origin in the atlas space	*p*-value of *F* (7, 7)	*p*-value of *F* (7, 7) at (*x*, *y*, *z*) locations
Olfactory bulbs	4.52 ± 0.03	0.0032	0.0551, 0.0032, 0.0004
Basal ganglia left	2.93 ± 0.02	0.0003	0.0360, 0.0237, 0.0003
Basal ganglia right	2.91 ± 0.02	0.0004	0.4858, 0.0073, 0.0094
Anterior commissure	2.14 ± 0.03	0.0416	0.6973, 0.0368, 0.0000
Fimbria of hippocampus	2.25 ± 0.03	0.0023	0.1768, 0.0128, 0.0000
Mammillary body	0.57 ± 0.04	0.0016	0.4267, 0.0011, 0.0019
Substantia nigra left	1.82 ± 0.02	0.0000	0.0056, 0.0002, 0.0000
Substantia nigra right	1.83 ± 0.03	0.0001	0.0003, 0.0001, 0.0001
Superior colliculus	3.21 ± 0.01	0.0000	0.0054, 0.0053, 0.0000
Inferior colliculus	3.04 ± 0.04	0.0008	0.0019, 0.0064, 0.0073
Cerebellum	2.62 ± 0.01	0.0000	0.0013, 0.5836, 0.0777

The absolute distances from the origin are shown as mean ± SD (in mm). The origin is at posterior end of the interpeduncular fossa (*O*). *F*-tests were performed to test the null hypothesis that the variances in the atlas space are less than those in the native space. Variations in absolute distance (*middle column*) and in coordinate (*right column*) were both examined

Table 3 Volumes of the structures retrieved from the native and the atlas probability map at different thresholds

	Threshold = 100%		Threshold = 87.5%		Threshold = 62.5%	
	Native	Atlas	Native	Atlas	Native	Atlas
Olfactory bulbs	0.00%	70.86%	53.06%	81.94%	85.14%	94.93%
Cerebrum	72.70%	92.43%	83.48%	95.42%	97.10%	99.06%
Basal ganglia	46.68%	73.64%	60.66%	84.18%	94.00%	96.97%
Anterior commissure	2.02%	20.81%	4.77%	48.25%	34.75%	84.04%
Fimbria of hippocampus	0.00%	30.61%	0.13%	50.61%	27.83%	80.63%
Diencephalon	72.70%	88.55%	83.80%	93.18%	96.66%	98.75%
Mammillary body	0.00%	27.88%	0.00%	46.96%	76.35%	81.70%
Midbrain—hindbrain	62.40%	84.33%	80.55%	91.49%	95.01%	96.81%
Substantia nigra	0.39%	43.90%	5.86%	65.49%	56.73%	90.60%
Superior colliculus	7.33%	78.09%	47.96%	85.37%	81.60%	95.17%
Inferior colliculus	5.25%	46.64%	18.39%	71.88%	61.74%	92.54%
Cerebellum	14.84%	50.67%	43.58%	80.73%	79.04%	93.74%

Values were normalized to the average volume of the corresponding structures. The volumes retrieved with threshold at 62.5% were at least 90% of the average size for main anatomical structures. Retrieved volumes for all other smaller structures were more then 80% of the average atlas volume. Surface models for the label volumes retrieved with this probability threshold were shown in Fig. 6

parameter transformation. This brought the MRI volume into the shape of the brain assuming only linear distortions were introduced while preparing the histological sections. Correction for the 2D nonlinear distortion was then performed by warping the histological images to their corresponding MR images using a continuum-mechanical warping algorithm (Thompson and Toga 1998). A 3D image volume from a single animal was then constructed using 150 registered histological sections, each of which was 50 μm apart from the neighboring sections. The height (y) of the volume was determined by the distance between serial images, and the width (x) and depth (z) were determined by the camera's field of view.

Tissue labeling for the histological image volume was performed following correction for 2D nonlinear distortion. In the previous work, 145 anatomical structures were delineated using Paxinos' atlas for adult mouse brain (2001) and Schambra's atlas for embryonic mouse brain (1992) as references (unpublished data). The delineation was based on coronal sections, aided by the other two orthogonal planes. The relationships between anatomical structures were organized hierarchically. The anatomically labeled volume used for feature-based registration and morphometrical analysis was reconstructed from these delineations based on the defined hierarchical relations. The resulting labeled brain volume contained exactly the same anatomical labels as the proposed atlas. Boundaries of the structures listed in our atlas are easily identified in the histological images.

Matching test between the atlas and test brains

The labels of the atlas and the test brain were superimposed in 3D. The volumes of match/mismatch for each structure were then computed. The sensitivity was described as the percentage of a test anatomical label falling into the corresponding atlas anatomical label space (i.e. being mapped with correct atlas label). The error rate was defined as the percentage of an atlas anatomical label falling outside of the corresponding anatomical label space of the test brain (i.e. the atlas mapped onto a structure inaccurately).

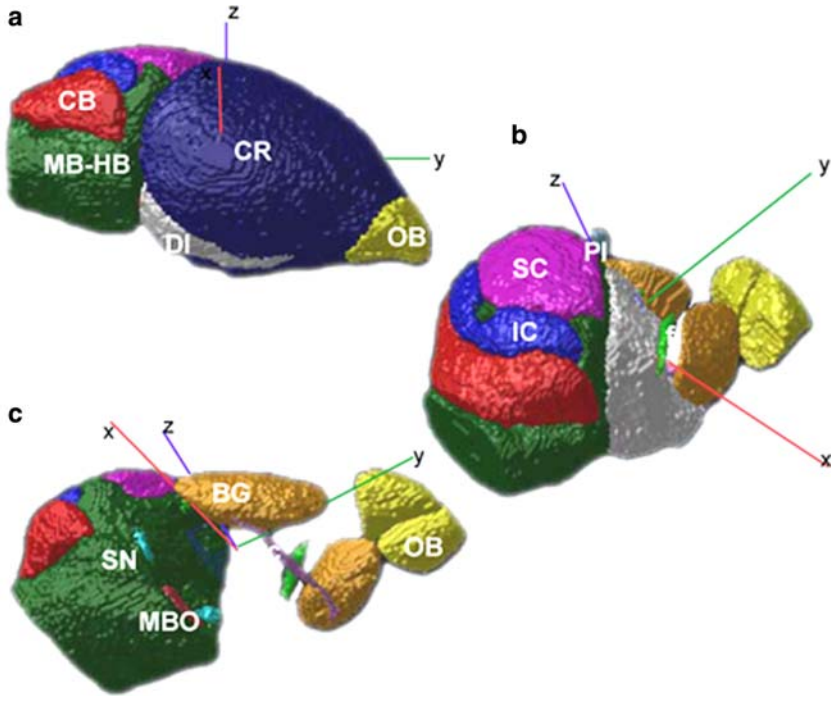

Fig. 6 Surface models of anatomical structures retrieved from the probability anatomical map at threshold equal to 62.5%. The volumes retrieved with threshold at 62.5% were at least 90% of the average size for main anatomical structures (structures shown in *bold* in Table 3). Retrieved volumes for all other smaller structures were more than 80% of the average volume. **a** OB (*yellow*): olfactory bulbs. CR (*dark*) blue: cerebrum. DI (*white*): diencephalon. MB-HB (*dark green*): midbrain–hindbrain. CB (*red*): cerebellum. SC (*magenta*): superior colliculus. IC(*blue*): inferior colliculus. BG (*orange*): basal ganglia. f (*green*): fimbria of hippocampus. AC (*pink*): temporal limb of AC. SN (*cyan*): substantia nigra. MBO (*light red*): mammillary body. PI (*light blue*): pineal gland. **b** surface of cerebrum was removed. **c** surfaces of cerebrum and diencephalon were removed

Results

Construction of atlas space

The average image volume of the eight co-registered brains provided resolution equivalent to the individual images (selected views in Figs. 4b, 5). Boundaries of olfactory bulb, cerebrum, diencephalon, midbrain—hindbrain, and cerebrum could be clearly discriminated in this average image volume. Caudate putamen and globus pallidus, mammillary bodies, superior and inferior colliculi, substantia nigra, and white matter tracts AC and fimbria of hippocampus were also identifiable. After co-registration, the *y*-axis (OI lines in Figs. 1, 3) rotated 0.03° from the horizontal plane on average (pitch, roll, yaw: $0.03 \pm 0.01, 0.00 \pm 0.00, 0.00 \pm 0.00$, respectively). By measuring the distances between landmarks, we found the average *x*, *z*, *y* scale, dimension change −1.96, −14.23 (not statistically significant at $p = 0.05$), and +2.26%, respectively after co-registration (Table 1). No strong relationship was found between the sizes of the brains and the subject weights ($R = 0.4949$). Brain sizes in atlas space were not different from native space (*t*-test, $p > 0.05$), while the variation in volume was reduced after transforming to the atlas space (*F*-test, $df = (7, 7)$, $p < 0.05$).

Excepting basal ganglia, anatomically labeled volumes were the same in the atlas space and native space (*t*-test, $p > 0.05$) (Table 1). Variations in the volumes of olfactory bulbs, cerebrum, and diencephalon were reduced after registering to the standard space (*F*-test, $df = (7, 7)$, $p < 0.05$, Table 1). Variation was also reduced in the cerebellum, although not significantly. Variations in the displacement of some features at the extrema of brain at each dimensions and in the distance of center-of-masses of several structures from the origin were much less in the atlas space (Tables 1, 2, distance), suggesting that the co-registration steps normalized each anatomical structure regionally. We also analyzed the variation in center-of-mass at each *x*, *y*, and *z* directions (Table 2, variance in co-ordinate). Variations were reduced primarily in *y* and *z* directions for all structures except the cerebellum. Reduction of variation in the *x*-direction was less prominent.

Probability maps constructed before and after registration were compared (Table 3). Selected views of the probability map for anatomical structures in the atlas space are shown in Fig. 5. All structures could be retrieved from the atlas map with high probability. Whereas retrieving from the native map failed for some small structures with high thresholds (100 and 87.5%). Boundaries of the olfactory bulbs, cerebrum, diencephalon, midbrain—hindbrain, and cerebellum were close to those of the label volume retrieved at probability threshold equal to 62.5% (areas with color red, orange,

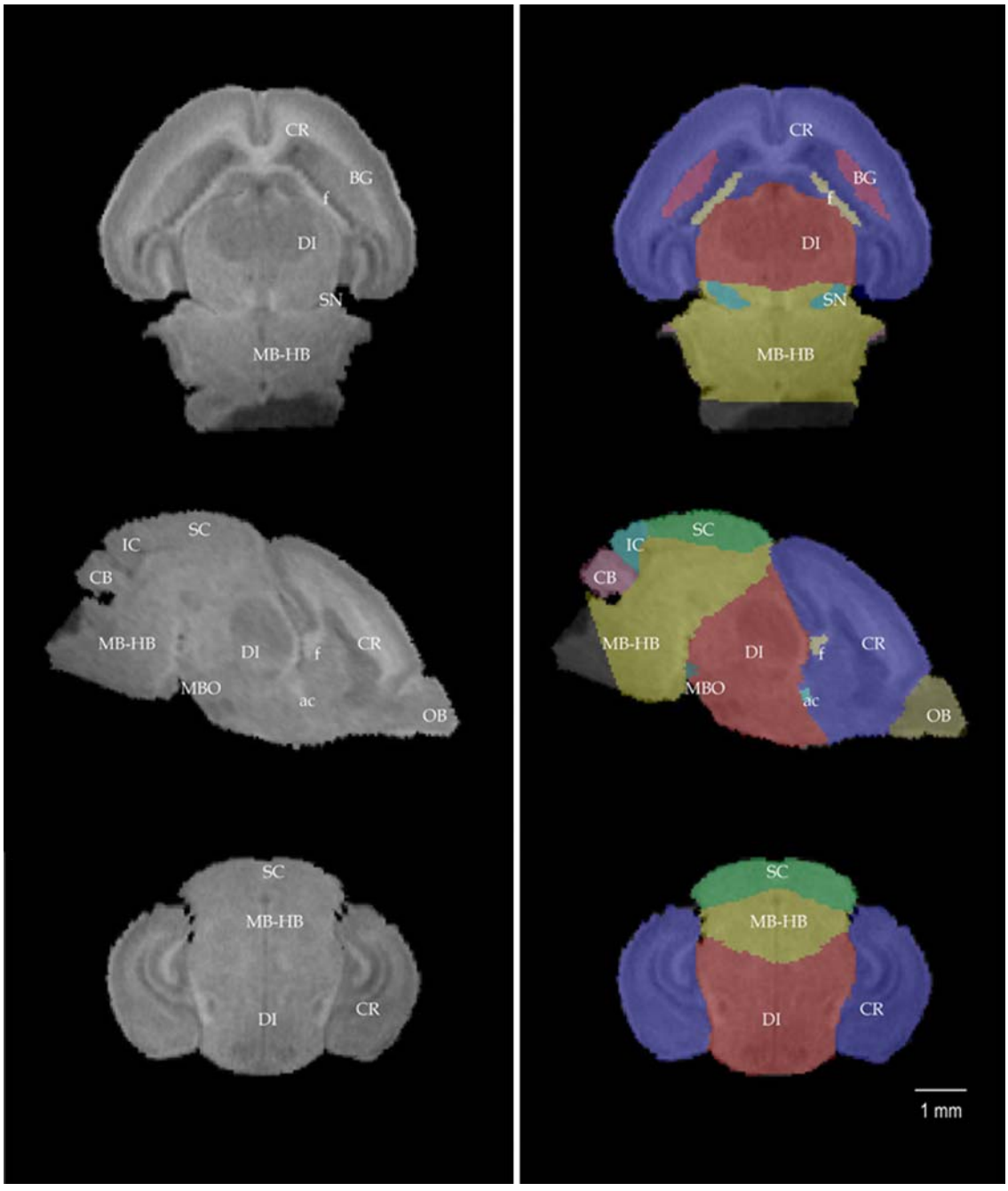

Fig. 7 Anatomical delineation for the test MR brain using the atlas as reference. The test brain is a T1-weighted MR data from a subject which was not used to construct the atlas. Labeling was performed after the brain was registered to the atlas brain image using a 12-parameter transformation. *Left column* shows the brain image without labels overlapping. View shown here was sampled at an approximate location as shown in Fig. 2. *Rows* from top to bottom: horizontal, sagittal, and coronal views

and yellow on Fig. 5a). The volumes retrieved with a threshold of 62.5% were at least 90% of the average size for main anatomical structures (structures shown in bold in Table 3). Retrieved volumes for all other smaller structures were more than 80% of the average atlas volume (Fig. 5b). Surface models for the label volumes retrieved with the probability threshold equal to 62.5% were shown in Fig. 6.

A general application

The T1-weighted MR image volume used for testing was acquired from a P0 mouse brain of another dame, but due to fewer siblings and possibly also a different protocol used to process the brain, it was 1.42 times the average size of the brains used to construct the atlas. The purpose of using this brain was to examine the gener-

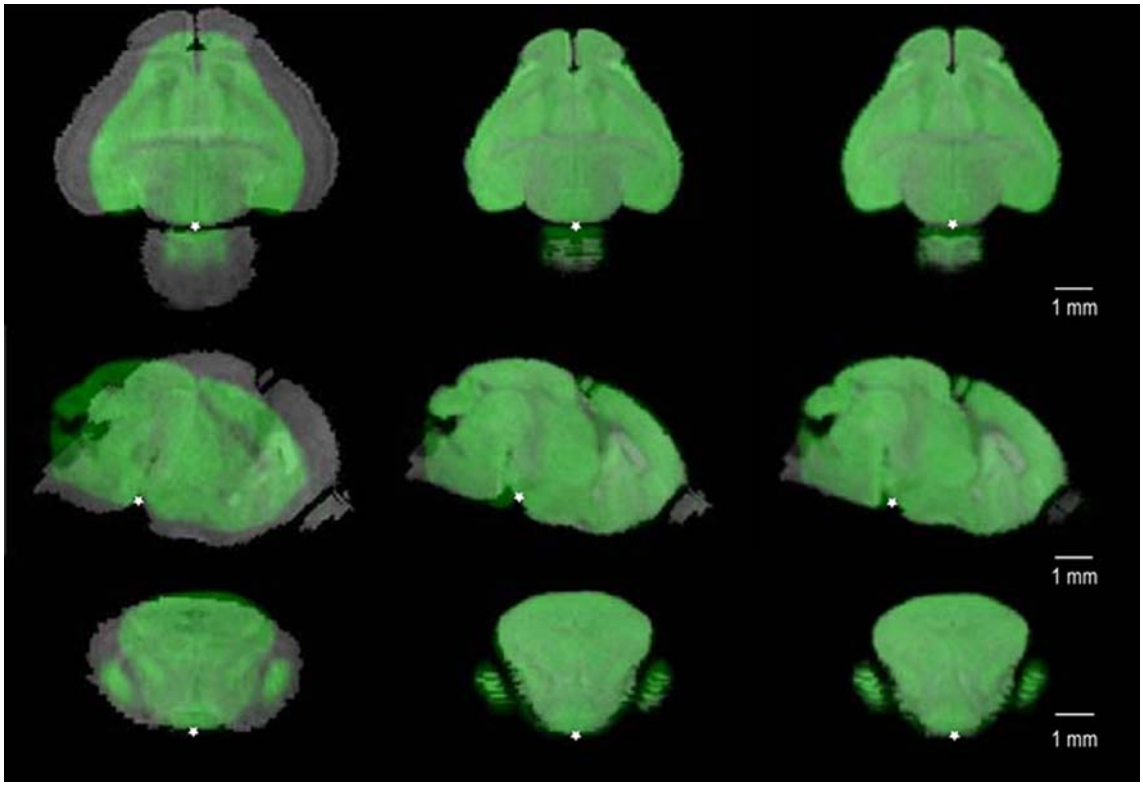

Fig. 8 The registration results of the test MR image volume of registration step were superimposed with atlas brain volume (*green*). The view was sampled at the origin (shown as *white dots*, coordinate (0, 0, 0)). *Columns* from left to right are the registration results of six-parameter transformation, additional 12-parameter transformation, and the final feature-based nonlinear warping. *Rows* from top to bottom: the horizontal, sagittal, and coronal views

alization of the atlas framework for serving a protocol-independent template. Initially, normalization could be achieved with a 12-parameter transformation when the atlas brain image served as a registration target (middle column of Fig. 8). Another feature-based warping (using the 13 anatomical labels described in the atlas) (Figs. 2, 7) further registered the brain to the atlas space (right column of Fig. 8). Degrees of pitch, roll, and yaw of the test brain after registering to the atlas space were consistent with those of the atlas brain (0.02, 0.00, and 0.00). Except for the cerebellum, the distance between the center-of-masses and the origin were within the predicted confidence ranges ($\pm$ t (0.025, 7) $\times$ S.D. of the values of the structures from the brains used to define the atlas space), suggesting spatial normalization was achieved in these structures (Table 4). The revised anatomical labels based on the intensity-average brain and the anatomical labels collected from the probability map at a threshold of 62.5% were both used to perform a tissue-matching test (Table 5). No obvious difference was observed in the sensitivities using these two types of label maps for structures with large volume-to-area ratios, suggesting that the label space retrieved from the probability map at a threshold equal to 62.5% provided a mapping essentially the same as the revised labels based on the average brain for these structures. Statistical testing showed a possible correlation between the sensitivity of the label space retrieved from the probability map at a threshold equal to 62.5% and the volume-to-surface area ratio (V/A) of the structure (Tables 5, 6, $R^2 = 0.7384$ for sensitivity to log (V/A) for the atlas anatomical structures retrieved from the probability map at threshold = 62.5%). Sensitivities were lower in structures with smaller V/A ratio, such as

Table 4 Registration results were examined using the absolute distance (in mm) between the center-of-masses and the origin

Structure	Predicted confidence range	Test brain deviated from the atlas
Olfactory bulbs	±0.08	−0.03
Basal ganglia left	±0.04	0.02
Basal ganglia right	±0.05	0.03
Anterior commissure	±0.07	−0.00
Fimbria of hippocampus	±0.08	−0.02
Mammillary body	±0.10	−0.01
Substantia nigra left	±0.05	0.02
Substantia nigra right	±0.07	0.06
Superior colliculus	±0.02	0.01
Inferior colliculus	±0.10	0.02
Cerebellum	±0.01	0.02

Confidence ranges were calculated by $\pm t$ (0.025, 7) $\times$ SD of the values of the structures of the brains used to defined the atlas space (left column). *Right column* shows the difference between the registered test brain and the atlas average

Table 5 Sensitivities (the percentage that the testing structural volumes falling within the ranges of their corresponding atlas labels) and error rates (percentage of incorrect mapping) of the atlas labels based on the average brain and the atlas labels retrieved from the probability map at threshold = 62.5%

Anatomical labels	Revised labels based on the average brain		Retrieved from the probability map at threshold = 62.5%	
	Sensitivity	Error rate	Sensitivity	Error rate
Olfactory bulbs	84.27%	9.69%	84.94%	11.36%
Cerebrum	98.06%	4.70%	98.05%	5.40%
Basal ganglia	97.13%	23.60%	97.61%	24.93%
Anterior commissure	81.77%	52.92%	73.31%	47.19%
Fimbria of hippocampus	68.33%	23.31%	60.41%	20.39%
Diencephalon	98.06%	7.72%	97.31%	6.36%
Mammillary body	75.53%	28.71%	67.97%	13.89%
Midbrain–hindbrain	95.77%	9.02%	96.70%	9.93%
Substantia nigra	87.74%	44.40%	87.12%	43.20%
Superior colliculus	93.74%	10.25%	93.19%	11.23%
Inferior colliculus	93.33%	23.50%	94.69%	25.58%
Cerebellum	95.89%	14.33%	96.15%	14.66%

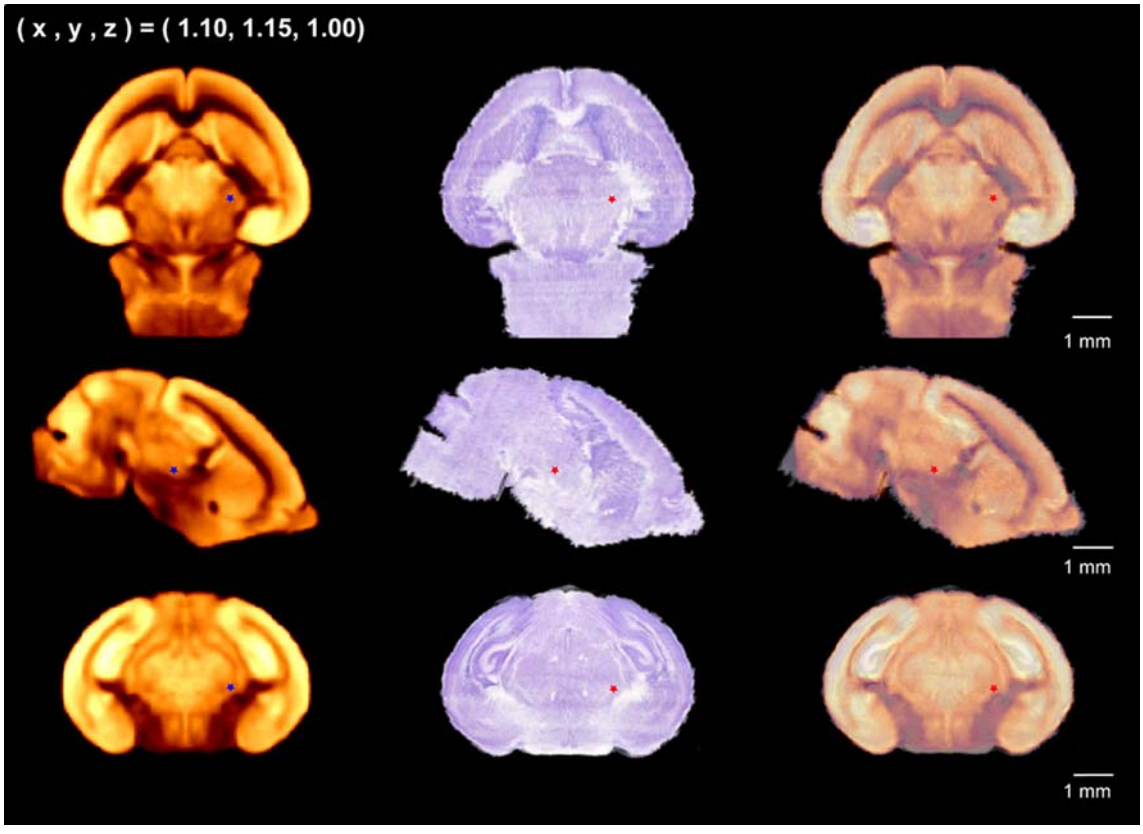

Fig. 9 The reconstructed histological stained brain was registered to the atlas space. View was sampled at coordinate (1.10, 1.15, 1.00) (in mm, shown as dots on the brain images). From left to right: the intensity average of co-registered MRI, the histological image volume registered to the atlas space, and the overlap of the images at the two left volumes. Rows from top to bottom: horizontal, sagittal, and coronal views

the white matter tracts and the mammillary bodies. Although the sensitivity of the label space retrieved from the probability map at a threshold of 62.5% was not as good as the revised label space for structures with small V/A ratio, the error rate of the former was lower. We also noticed that the error rate was related to the clarity of boundaries of the corresponding structures.

Cross validation with histological data

We also examined whether the atlas framework is applicable for the brain volume reconstructed from histological images. Since the histological staining revealed a detailed cytoarchitecture of the brain, the stained brain images could provide a high-resolution

Table 6 Volume/surface ratios (mm) of the anatomical labels retrieved from the probability map at threshold = 62.5%

	Volume/surface
Olfactory bulbs	0.16
Cerebrum	0.50
Basal ganglia	0.20
Anterior Commissure	0.05
Fimbria of hippocampus	0.05
Diencephalon	0.39
Mammillary body	0.06
Midbrain—hindbrain	0.43
Substantia nigra	0.08
Superior colliculus	0.19
Inferior colliculus	0.14
Cerebellum	0.19

anatomical map if a standard coordinate system was applied. After registering to the atlas space, pitch, roll, and yaw degrees of the histological brain are 0.05, −0.01, and −0.01 from the atlas space (Fig. 9). Deviation in the direction of *y*-axis (pitch 0.05) resulted in positive deviations in the center-of-mass in the *z*-direction for structures whose coordinates are positive in both *y* and *z* directions (Table 7). The OI line defined in Fig. 1 was 4.36% less than the population average length in the atlas. As a result, structures whose center-of-masses located in the positive/negative direction of the *y*-axis negatively/positively deviated from the atlas. The differences in the volumes of cerebrum, diencephalon, and midbrain–hindbrain from the average anatomical space were −4.57, 3.61, and −2.35% of the volumes of the corresponding structures in the atlas, but only the difference in cerebrum was statistically significant ($p < 0.05$) (Table 8). The differences (normalized to the corresponding volume) in the volumes of the substructures from the atlas space were either larger or about the same as those of the larger structures containing them. While local nonlinear distortion in the histological image volume was minimized with feature-based warping, the inconsistencies in the proportions of structural size within the same segment of the brain mostly resulted from the conservative decisions made when labeling the low-resolution MR images. With histological staining, boundaries of these anatomical structures could be identified more accurately, thereby providing an anatomical reference more confidently.

To evaluate the applicability of atlas-based mapping for the histological brain, we applied the probability atlas to this high-resolution image volume and examined the mapping accuracy of the label retrieved at the threshold 62.5% (red and orange area in right column of Fig. 10). As in the case applying to the MRI test brain, the sensitivity for histological images was related to V/A of the structure of the atlas (Tables 6 and 9 using all labels in the atlas, $R^2 = 0.8373$ for sensitivity to log (V/A) of the atlas anatomical labels). The atlas did not provide a sensitivity as good as it could offer the image volumes obtained with non-invasive methods. On the other hand, mapping error rates were less influenced by data acquisition methods when compared with the results using MRI volume as the test brain (Tables 5, 9 using all labels in the atlas).

From the results of morphometrical analysis, we considered that the distortion of the reconstructed histological brain might be beyond what a native atlas space could capture. Therefore, instead, we were interested in whether local registration could be improved if we avoided global normalization. We, thus, modified the registration strategy by using only some of the anatomical structures defined in the atlas for feature-based registration. One approach used a label volume that excluded the olfactory bulbs and the cerebellum, which are structures most susceptible to physical distortions in the absence of the skull. Another approach used a label volume that excluded the cerebrum, diencephalon, and the midbrain–hindbrain, relaxing the restraint of these structures on brain shape. Mapping accuracies of the probability atlas (threshold at 62.5%) for the registered test brains were then examined (Table 9). Either an increase in sensitivity or a decrease in error rate of the atlas, or both, was achieved in structures used for feature-based registration. Higher error rates for the inferior colliculus when the cerebellum was not used,

Table 7 Differences in *x*, *y*, *z* locations of center-of-masses of the structures in the histological brain from the population average (in mm) after registering to the atlas space

	Predicted confidence interval	Displacement of centers from the atlas space
Olfactory bulbs	±0.03, ±0.07, ±0.04	−0.03, −0.04, 0.09
Basal ganglia left	±0.06, ±0.07, ±0.06	−0.09, −0.07, 0.12
Basal ganglia right	±0.08, ±0.08, ±0.07	0.10, −0.09, 0.15
Anterior commissure	±0.14, ±0.07, ±0.02	−0.00, −0.08, 0.07
Fimbria of hippocampus	±0.10, ±0.09, ±0.03	−0.02, −0.05, 0.07
Pineal gland	±0.06, ±0.21, ±0.13	0.02, −0.12, 0.15
Mammillary body	±0.05, ±0.05, ±0.10	0.10, 0.09, 0.17
Substantia nigra left	±0.03, ±0.04, ±0.05	0.02, 0.07, 0.10
Substantia nigra right	±0.03, ±0.04, ±0.08	0.02, 0.05, 0.13
Superior colliculus	±0.03, ±0.14, ±0.01	−0.03, 0.06, −0.02
Inferior colliculus	±0.04, ±0.17, ±0.15	0.04, 0.19, 0.00
Cerebellum	±0.06, ±0.35, ±0.45	−0.06, −0.03, 0.05

Predicted confidence interval (*middle column*) was defined by the range $\pm t(0.025, 7) \times$ SD of the volumes of the structures of the brains used to construct the atlas space. *Right column* shows the difference between the histological brain and the atlas average

Table 8 Differences in the volumes of the structures of the registered histological brain from the population average

	Predicted interval ($p = 0.05$)	Difference from the atlas
Olfactory bulbs	±12.04%	22.36%
Cerebrum	±2.57%	−4.57%
Basal ganglia left	±15.57%	22.77%
Basal ganglia right	±12.40%	28.27%
Anterior commissure	±42.32%	45.76%
Fimbria of hippocampus	±19.52%	55.96%
Diencephalon	±3.75%	3.61%
Mammillary body	±73.64%	406.80%
Midbrain–hindbrain	±15.39%	−2.35%
Substantia nigra left	±39.37%	30.48%
Substantia nigra right	±31.62%	13.51%
Superior colliculus	±17.50%	−0.51%
Inferior colliculus	±14.53%	6.95%
Cerebellum	±15.36%	−15.92%
Brain	±5.63%	−2.66%

Differences were normalized to the corresponding average size of the atlas and shown as percentage. Predicted confidence interval was defined by the range $\pm t(0.025, 7) \times \mathrm{SD}$ of the values of the structures of the brains used to construct atlas space (normalized to the corresponding average size)

and lower sensitivity for the olfactory bulbs when the cerebrum was not used for feature-based registration suggested that the use of features close to the region of interest improves local registrations.

Discussion

Subject variation

Several factors make it difficult to establish a perfect atlas for neonatal mouse brains. One is due to the inherent variations between subjects. The animals were genetically identical and collected at the same gestational age. However, health conditions of the mother, the number of siblings, and environmental factors can result in different growth rates between subjects, especially between those from different litters. Since brains are undergoing massive volume expansion at this stage, minor differences in growth rates could result in significant variations in brain size. Therefore, the coordinate system defined by absolute scales used in adult mouse brain atlases is not suitable for the atlases of neonates. Instead, a coordinate frame independent of brain size is needed for brains not yet fully matured. Our P0 atlas provides a template for normalization. The coordinate values are assigned based on the atlas space and thus are independent of the morphological variation of the brain. We showed that variations in each dimension as well as in brain volumes were significantly reduced after registering to the atlas space, suggesting that the brains were normalized to a space that represents the brain geometry more consistently (Table 1). Moreover, the template brain was constructed by averaging image intensities of the co-registered brains, thus avoiding possible anatomical outliers present in one animal. As shown in Fig. 5, the areas with low probability in the anatomical probability map were not within the range of the corresponding structures on the image of the average brain.

The midbrain–hindbrain was the only structure whose variation in volume was not reduced in atlas space (Table 1). The variation in the volume of the midbrain–hindbrain region was significantly impacted by the lack of a clear boundary between the medulla and the midbrain–hindbrain. Variations in size of most anatomical structures we examined were reduced in the atlas space, suggesting that the normalization steps provided a reasonable anatomical framework. Not sur-

Table 9 Mapping accuracy of the atlas retrieved from the probability map with threshold at 62.5% for the registered histological brain

Feature used in registration	All in the atlas		Without OB and CB		Without CR, DI, and MBHB	
	Sensitivity	Error rate	Sensitivity	Error rate	Sensitivity	Error rate
Olfactory bulbs	70.02%	6.70%	**75.26%**	**6.51%**	64.04%	1.09%
Cerebrum	97.76%	7.75%	97.96%	7.09%	**95.83%**	**8.96%**
Basal ganglia	69.30%	12.68%	71.53%	12.12%	77.41%	4.40%
Anterior commissure	37.32%	37.90%	38.74%	35.65%	42.64%	16.04%
Fimbria of hippocampus	24.38%	51.52%	29.56%	44.94%	34.53%	24.08%
Diencephalon	85.80%	9.00%	87.37%	7.80%	**81.54%**	**12.44%**
Mammillary body	12.53%	20.02%	13.51%	15.72%	13.95%	9.58%
Midbrain–hindbrain	90.71%	9.12%	92.48%	8.38%	**88.68%**	**11.91%**
Substantia nigra	48.33%	33.28%	53.72%	29.59%	60.66%	20.69%
Superior colliculus	88.11%	12.03%	89.94%	11.71%	88.33%	10.47%
Inferior colliculus	70.97%	16.96%	73.71%	19.25%	74.83%	14.17%
Cerebellum	87.69%	24.01%	**81.40%**	**27.65%**	86.32%	13.34%

Percentage of the test brain volumes falling in the range of the atlas space (sensitivity) and the atlas labels falling outside the test brain (error rate) are used to evaluate the mapping accuracy. Alternative approaches for feature-based registrations were also taken by using the anatomical labels without the olfactory bulbs (*OB*) and the cerebellum (*CB*), and the labels without the cerebrum (*CR*), diencephalon (*DI*), and the midbrain–hindbrain (MB–HB). Results for the structures not used for feature-based registration are given in bold

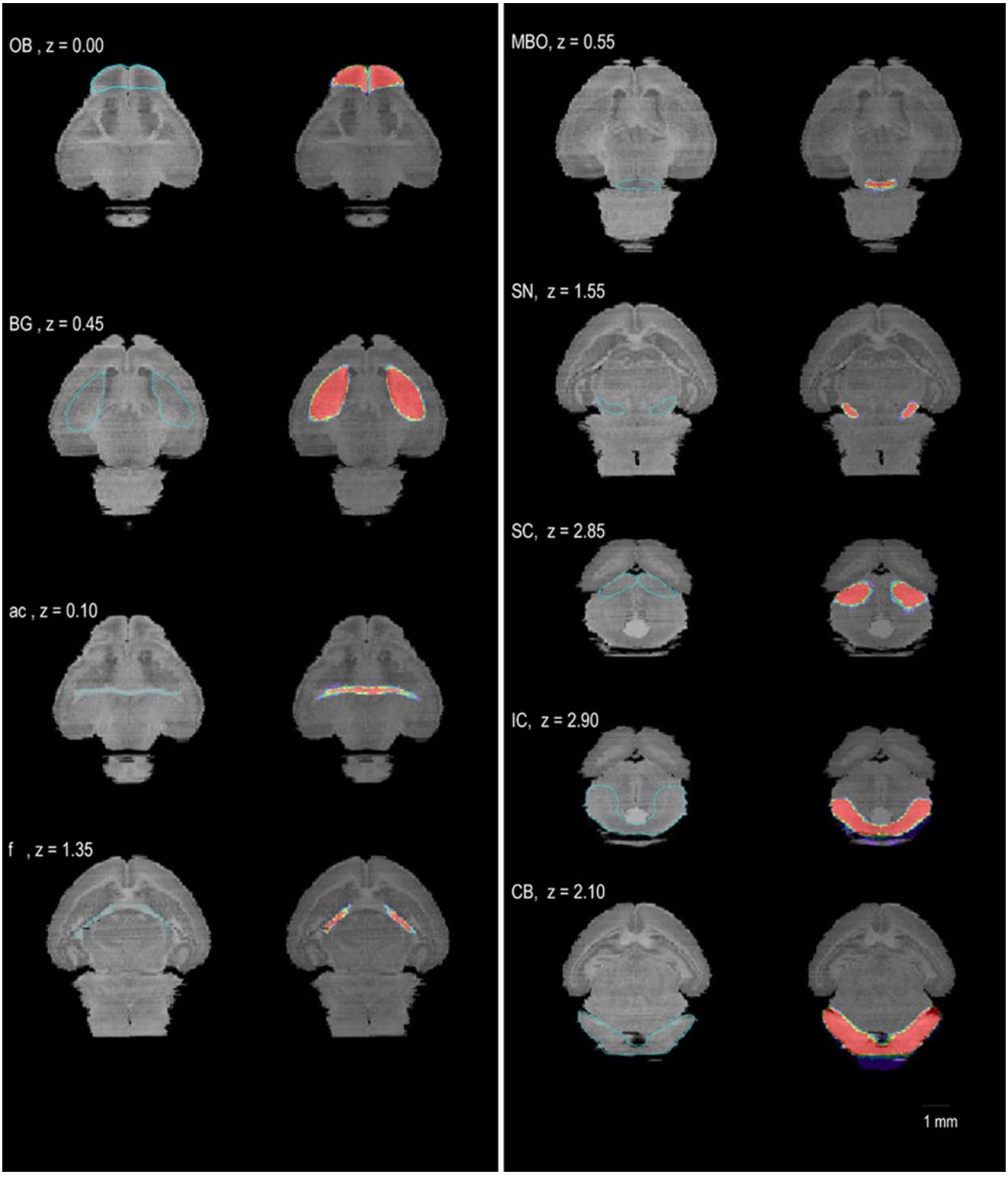

Fig. 10 Reconstructed Nissl-stained brain image volume registered to the atlas space. Each pair of the images shows one anatomical structure. Structures recognized on Nissl-stained images were outlined (left images) and the right images were superimposed with the corresponding probability maps of the atlas. *Z*-values indicate the atlas *z*-coordinates (in mm)

prisingly, we found that the amount of variation that could be decreased is related to how well the boundaries of the structures could be distinguished. The boundaries of these structures in MRI images were not always very clear; therefore, the variations in the size of anatomically labeled volumes might contain errors incurred while labeling the data, and thus unrelated to the variation between subjects.

Geometric variation

Since the skull, at early developmental stages, was not yet fully calcified, soft tissue is susceptible to mechanical forces encountered during sample preparations. Physical deformations during sample preparation can introduce nonlinear spatial variation. In addition, without a solid skull to hold the brain in a fixed position, structures at different sides of the flexures might adopt different relative positions. Although in theory, morphological differences within an inbred strain are low, linear, and proportion to brain size, these other factors make linear registration using internal landmarks inadequate to provide a stable framework.

Using the variations in center-of-mass of the anatomical structures in each x, y, and z dimensions, we could examine how the anatomical locations varied (Table 2, coordinate). Structures at the rostral and caudal extreme, like the olfactory bulbs and the cerebellum might articulate differently relative to the cerebrum, resulting in considerable spatial variations, particularly in the y and z directions. The resulting spatial variation could be reduced with feature-based nonlinear registrations. The anatomical features we used were structural labels selected from each segment of the brain (Fig. 2), and all of these structures provided part of the boundaries for the segments. Since the boundaries provided restrictions in structural locations, additional steps of nonlinear feature-based warping thus further improved registration results. By maximizing the mutual information of the anatomical label volumes between subjects, we successfully reduced the spatial variation in these two dimensions (y, z) in most structures since each segment of brain was warped to its geometrical average location. Increases in retrieved volume from the probability map with high-threshold shows the improvement in regional registration (Table 3).

Variation caused by labeling error

The most difficult problem in defining an accurate atlas space for neonatal brains resulted from the technical limitation in image acquisition. The maximum dimension of the mouse brain at P0 is between 5 and 8 mm (Fig. 4), while the best MR imaging resolution in this study was $0.04\times0.04\times0.04$ mm^3/voxel. Measurement errors became inevitable since a small displacement in the voxel space might introduce significant variations in world space. The normal mouse brain is bilaterally symmetric. Hence, the amount of labeling error can be estimated from the deviation of center-of-mass of symmetric structures about the medial sagittal plane. The average deviations in the x-coordinates of center-of-masses from zero in all structures were less then 0.04 mm (Table 2, coordinate), which was sub-voxel. Image resolution limited the accuracy of boundary delineation and made small structures difficult to recognize in the MR images. Therefore, the volumes that could be retrieved from the probability map at high thresholds for structures with small V/S were much smaller than the corresponding average volumes (Table 3). When applied to brains other than those used to construct the atlas, sensitivities were also less for structures with small V/S (Tables 5, 9).

Application to images acquired using non-invasive methods

Intensity contrast and resolution among structures vary depending on the image acquisition methods. Therefore, cross-modality registration is less satisfactory if the image intensity was used as the only optimization criterion. In our experiment using the T1-weighted MR image as the test subject, the brain image alone could serve as global normalization target. However, as the cross-correlation in intensity between the test and atlas images is low, good results in regional registration may not be achieved (Fig. 8, middle column). Additional feature-based registration thus further enables protocol-independent applications. Most of the anatomical structures defined in the atlas are discriminable visually without difficulty and provided boundaries for each segment of the brain. Therefore, these labels are good candidates for registration. In our experiment using images acquired with other non-invasive protocols (T1-weighted MR scan) as test brains, global and regional registrations to the atlas were achieved along with feature-based warping (Fig. 8 and Table 4), suggesting that the anatomical labels drawn on the intensity-averaged brain provided a stable framework for this unique non-littermate brain. The registration result can also be examined with the matching test, which showed the proportions of the test brain being correctly mapped by the atlas (Table 5, sensitivity). For structures whose volume/surface area ratios are larger than 0.2 mm, the atlas anatomical labels (Table 5, 6) could map 90% of their space correctly. Comparing with the result using the labels drawn on the average brain and labels retrieved from the probability maps with threshold at 62.6%, we found the later provided equivalent sensitivity but lower error rate for anatomical mapping (Tables 4, 5, 6). Since the revised labeled brain was delineated based on the average brain, it included additional uncertain boundary regions other than the probability map at a threshold of 62.5%. From this experiment, it is clear that while the revised labeled brain was required as the registration template without separated boundaries, the label spaces provided by probability map at a more restrictive threshold were more precise as a mapping reference.

Using the standard atlas space to evaluate the distortion in the histological data

A feature-based registration was used to warp the histological brain to an average native position. However, since the native shape of the brain was not well preserved after removal of the skull, the registration results

were not as good as those obtained by applying the atlas to images acquired using non-invasive methods. Deviations in the resulting morphometrics from the standard space implied that the geometric variations are beyond what the normal average could present, and thus could be used to evaluate the distortions incurred after the brain was removed from the skull. The resulting OI line of our test brain deviated from the horizontal plane of the atlas when maximum mutual information was achieved. Without the constraint provided by the skull, the fissures separating each segment of the brain make the anatomical structures take a relative location different from the native one. We found that structures located in the midbrain–hindbrain deviated less from the predicated range in the *z*-direction (Table 7). This suggests that the anatomical structures in the midbrain–hindbrain area used for feature-based warping were less susceptible to the distortion when the skull is absent, probably due to their anatomical locations.

Variations in the cellular architecture of different anatomical structures also introduced local nonlinear distortions. As sectioning was required for staining, slices containing structures with higher cell density are more sensitive to osmotic tension during mounting and staining. Among the brain segments (olfactory bulbs, cerebrum, diencephalon, midbrain—hindbrain, and cerebellum), the cell density is comparatively higher in the olfactory bulbs and lower in the cerebellum at P0. The histological brain in this study was cut coronally (cutting angle perpendicular to longitudinal axis). Small areas of the coronal sections in the olfactory bulbs/cerebellum allow the cell-density effect to become significant since it includes larger proportions of structures with high/low cell-density. This difference may cause the inconsistency in expansion/shrinkage across the longitudinal sections during sample preparation, and thus impairing the normalization after volume reconstruction (Table 8).

Cross validation of the anatomical delineations between the atlas and the high-resolution data

Labeling errors of the atlas anatomical structures could be inferred from the reconstructed histological atlas. Cross mapping between the atlas and the histological spaces showed that although most of the atlas anatomical labels were mapped onto the correct substructure in the histological space, the atlas did not label the histological image throughout the corresponding structures (Table 9 and Fig. 10). This effect occurred mainly in the substructures whose volumes were larger in the histological space than their counterpart in the atlas space (Tables 8, 9). The anatomical labels were arranged in a hierarchical relationship. When a voxel could not be correctly labeled with confidence, it was assigned to a structure at a corresponding coarser level that guarantees its inclusion (using the nomenclature tables in Swanson 1998). Hence, for images with lower resolution, the anatomical labels for structures with blurred boundaries always contained a smaller area than in the higher resolution data. The purpose of doing this was to avoid assigning a space incorrectly, at the cost of sensitivity. Larger volumes of the substructures in the histological space suggested that they included a larger area than what the atlas space defined.

Distortions introduced in the histological brain might cause it to deviate far away from its native shape. Therefore, global and regional registration criteria might not be achieved at the same time. Experiments using selected anatomical structures for feature-based registration demonstrated that regional registration was improved when the restriction of global normalization was relaxed (Table 9). Since histological staining differentiates the anatomical structures, with appropriate registration strategy, the anatomical space described in the high-resolution images can provide more boundary information for structures that could not be clearly identified in MR images. High-resolution gene expression maps are primarily generated using invasive methods. In order to map the anatomical space onto such data, feature-based co-registration with selected anatomical features in the neighborhood of the region of interest will provide more accurate results.

Conclusion

The atlas in this study provides an average brain image with a coordinate description, an anatomical label volume with 13 delineations (five regions and seven substructures), and probability maps for each of these structures to indicate the confidence range for anatomical mapping. The proposed atlas space in this study captured the average geometry of native anatomical space for normal mouse brains at P0. Although computationally intensive, nonlinear warping was a necessary registration step due to the inconsistent local distortions at this age. Feature-based registration limited the geometrical variation of the atlas, as the structures used for the template are spatially stable and consistent across subjects. Once a test subject is registered to the atlas space, the anatomical probability maps generated from the co-registered brains then can be used to predict the mapping accuracy. By selecting a threshold for the probability map, an anatomical space for each structure with various confidence intervals can be reconstructed. The probability map with a restrictive threshold provides a more accurate mapping, while the one with lower threshold labels an image more completely.

In addition to an anatomical map, the anatomical labeled brain based on the average brain image offers a template to facilitate cross-modality applications. By providing an anatomical framework, atlas-based registration also solves the mapping problem, which comes from the variation in morphology at early development stages.

Although the atlas based on MR images could not be presented as a detailed anatomical map as the one based

on invasive histological staining, it provided a native framework to house and standardize high-resolution data. In our ongoing work, the histologically stained P0 mouse brain has been delineated thoroughly (145 structures) and the anatomical database associated with it relates to the adult mouse brain atlas (MacKenzie-Graham et al. 2004). Presenting the high-resolution anatomy in the standard atlas space thus permits the integration and analysis of data from the different development stages both in spatial and temporal dimensions.

The atlas templates and the probability maps of the anatomical labels are available for download at http://www.loni.ucla.edu/MAP/. Tools for viewing, labeling, and registering images also are available at http://www.loni.ucla.edu/Software/.

Acknowledgments This work was supported by the NIBIB research grant R01 EB002172, the NCRR BIRN grant U24 RR021760, and the Beckman Institute at Caltech. Additional support was provided by the NCRR resource grant P41 RR013642 and the National Institutes of Health through the NIH Roadmap for Medical Research, Grant U54 RR021813 entitled Center for Computational Biology (CCB). Information on the National Centers for Biomedical Computing can be obtained from <http://nihroadmap.nih.gov/bioinformatics>.

References

Baldock R, Bard J, Brune R, Hill B, Kaufman M, Opstad K, Smith D, Stark M, Waterhouse A, Yang Y, Davidson D (2001) The Edinburgh mouse atlas: using the CD. Brief Bioinform 2:159–169

Chiavaras MM, LeGoualher G, Evans A, Petrides M (2001) Three-dimensional probabilistic atlas of the human orbitofrontal sulci in standardized stereotaxic space. Neuroimage 13:13479–13496

Diep DB, Hoen N, Backman M, Machon O, Krauss S (2004) Characterisation of the Wnt antagonists and their response to conditionally activated Wnt signalling in the developing mouse forebrain. Brain Res Dev Brain Res 153:261–270

Gray PA, Fu H, Luo P, Zhao Q, Yu J, Ferrari A, Tenzen T, Yuk DI, Tsung EF, Cai Z, Alberta JA, Cheng LP, Liu Y, Stenman JM, Valerius MT, Billings N, Kim HA, Greenberg ME, McMahon AP, Rowitch DH, Stiles CD, Ma Q (2004) Mouse brain organization revealed through direct genome-scale TF expression analysis. Science 306:2255–2257

Jacobowitz DM, Abbott LC (1998) Chemoarchitectonic atlas of the developing mouse brain. CRC Press, Boca Raton, FL

Kovacevic N, Henderson JT, Chan E, Lifshitz N, Bishop J, Evans AC, Henkelman RM, Chen XJ (2004) A three-dimensional MRI atlas of the mouse brain with estimates of the average and variability. Cereb Cortex. DOI 10.1093/cercor/bhh165

Leow A, Huang SC, Geng A, Becker J, Davis S,Toga AW, Thompson P (2005) Inverse consistent mapping in 3D deformable image registration: its construction and statistical properties. In: To appear in Proceedings of the IPMI (information processing in medical imaging).Glenwoods Springs, CO, pp11–15

Li DF, Freeman AW, Tran-Dinh H, Morris JG (2004) A cartesian co-ordinate system for human cerebral cortex. J Neurosci Methods 125:137–145

MacKenzie-Graham A, Lee EF, Dinov ID, Bota M, Shattuck DW, Ruffins S, Yuan H, Konstantinidis F, Pitiot A, Ding Y, Hu G, Jacobs RE, Toga AW (2004) A multimodal, multidimensional atlas of the C57BL/6 J mouse brain. J Anat 204:93–102

Mazziotta J, Toga A, Evans A, Fox P, Lancaster J, Zilles K, Woods R, Paus T, Simpson G, Pike B, Holmes C, Collins L, Thompson P, MacDonald D, Iacoboni M, Schormann T, Amunts K, Palomero-Gallagher N, Geyer S, Parsons L, Narr K, Kabani N, Le Goualher G, Boomsma D, Cannon T, Kawashima R, Mazoyer B (2001) A probabilistic atlas and reference system for the human brain: international consortium for brain mapping (ICBM). Philos Trans R Soc Lond B Biol Sci 356:1293–1322

Ourselin S, Roche A, Subsol G, Pennec X, Ayache N (2001) Reconstructing a 3D structure from serial histological sections. Image Vis Comput 19:25–31

Parras CM, Galli R, Britz O, Soares S, Galichet C, Battiste J, Johnson JE, Nakafuku M, Vescovi A, Guillemot F (2004) Mash1 specifies neurons and oligodendrocytes in the postnatal brain. EMBO J 23:4495–4505

Paxinos G, Franklin KJB (2001) The mouse brain in stereotaxic coordinates. Academic Press, San Diego, CA

Rehm K, Rottenberg SD, Schaper K, Sternt J, Hurdal M, Sumner DW (2000) Use of cerebellar landmarks to define a co-ordinate system and an isolation strategy. NeuroImage 11:S536

Schambra UB, Lauder JM, Silver J (1992) Atlas of the prenatal mouse brain. Academic Press, San Diego, CA

Shattuck DW, MacKenzie-Graham A, Toga AW (2004) DUFF: software tools for visualization and processing of neuroimaging data. Biomedical imaging: macro to nano. IEEE Int Symp 644A–647A

Swanson LW (1998) Brain maps: structure of the rat brain: a laboratory guide with printed and electronic templates for data, models, and schematics. Elsevier, Amsterdam

Talairach J, Tournoux P (1988) Co-planar stereotaxic atlas of the human brain. Thieme Medical, NY

Thompson PM, Toga AW (1998) Anatomically-driven strategies for high-dimensional brain image warping and pathology detection. In: Toga AW (ed) Brain warping. Academic Press, San Diego, CA, pp 311–336

Thompson PM, Mega MS, Toga AW (2002) Subpopulation brain atlases. In: Toga AW, Mazziotta JC (eds) Brain mapping: the methods. Academic Press, San Diego CA, pp 757–796

Toga AW, Santori EM, Hazani R, Ambach K (1995) A 3D digital map of rat brain. Brain Res Bull 38:77–85

Toga AW, Goldkorn A, Ambach K, Chao K, Quinn C, Yao P (1997) Postmortem cryosectioning as an anatomical reference for human brain mapping. Comput Med Imaging Graph 21:131–141

Watanabe H, Andersen F, Simonsen CZ, Evans SM, Gjedde A, Cumming P, DaNeX Study Group (2001) MR-based statistical atlas of the Gottingen minipig brain. Neuroimage 14:1089–1096

Woods RP, Mazziotta JC, Cherry SR (1993) MRI-PET registration with automated algorithm. J Comput Assist Tomogr 17:536–546